Gas Production from Methane Hydrate in a Pilot-Scale Hydrate Simulator Using the Huff and Puff Method by Experimental and Numerical Studies

Bo Li,[†] Gang Li,[†] Xiao-Sen Li,*,[†] Qing-Ping Li,[†] Bo Yang,[†] Yu Zhang,[†] and Zhao-Yang Chen[†]

[†]Key Laboratory of Renewable Energy and Gas Hydrate, Guangzhou Institute of Energy Conversion, Chinese Academy of Sciences, Guangzhou 510640, China

ABSTRACT: A novel three-dimensional 117.8-L pressure vessel, which is called a Pilot-Scale Hydrate Simulator (PHS), is developed to investigate the gas production performance from hydrate-bearing porous media using the huff and puff method through both experimental and numerical simulations. The methane gas and deionized water are injected into the pressure vessel to synthesize methane hydrate. The grain sizes of the quartz sand in the vessel are between 300 and 450 μm. The huff and puff stages, including the injection, the soaking, and the production, are employed for hydrate dissociation. A single vertical well at the axis of the PHS is used as the injection and production well. The whole experiment consists of 15 huff and puff cycles. The numerical simulation results agree well with the experiment. Both the experimental and numerical simulation results indicate that the injected water is mainly restricted around the well during the injection stage. The system pressure fluctuates regularly in each cycle, and the secondary hydrate is formed under the pressurization effect caused by the hot water injection in the injection stage. The gas production rate maintains approximately stable in a relatively long period. The sensitivity analysis indicates that the gas production can be enhanced with high intrinsic permeability of the deposit or by raising the temperature of the injected hot water. The mass of the water produced in each cycle has little difference and is manageable when using the huff and puff method.

1. INTRODUCTION

Natural gas hydrates (NGH) are crystalline compounds in which small guest molecules (such as CH_4, CO_2, H_2S, etc.) occupy the host lattices formed by water molecules. The majority of naturally occurring gas hydrates contain CH_4, and the amount of natural gases trapped in gas hydrates is estimated to be huge. Recent seismic explorations and geological researches show that natural gas hydrates exist widely in marine sediments and permafrost areas where the necessary conditions of low temperature and high pressure exist for hydrate stability.[1] It is thought to be a potential strategic energy resource that can replace the known conventional fossil fuel resources in the future.[2]

Decomposition of gas hydrate can be induced by shifting the thermodynamic equilibrium conditions. The following methods have been proposed: (1) depressurization,[3−5] in which the deposit pressure is set to be lower than the hydration pressure at the prevailing temperature; (2) thermal stimulation,[6−11] in which hot water or heat is injected into the deposit to raise the temperature above the dissociation temperature; (3) thermodynamic inhibitor injection,[12−14] in which the hydrate pressure−temperature equilibrium conditions are shifted by the use of chemicals, such as salts and alcohols. Another production method involves replacement of CH_4 in the hydrate by another hydrate-forming gas (e.g., CO_2) of which the equilibrium reaction conditions are more favorable.[15,16]

Recent studies have shown that gas production can be enhanced when depressurization is used in conjunction with thermal stimulation by hot water, hot brine, or steam injection with the vertical well.[17,18] The huff and puff method, also known as the cyclic steam stimulation (CSS), was accidentally discovered by the Shell Oil Company in 1960 and is widely used in the oil industry.[19,20] When used in gas production from hydrates, it is a special form of the combination of depressurization and thermal stimulation methods.

Recent numerical simulations have employed the huff and puff method to investigate into the gas production potential from marine and permafrost hydrate deposits.[21,22] A typical huff and puff cycle usually consists of three stages: injection, soaking, and production. During the injection stage, the hot water or steam is injected into the deposit from the well for a certain amount of time. Then the well is closed for some time in the soaking stage to allow heat diffusion. After that, the gas and water are pumped out of the deposit from the same well for a period of time. During the production stage, the well pressure will decrease continuously. When the pressure drops to a certain value, the next huff and puff cycle begins. It has been proved effective in gas production under suitable injection and production conditions.

To investigate the characteristics of hydrate decomposition in porous media of actual reservoir, one of the effective ways is to develop 3D experimental apparatus to simulate the hydrate dissociation process. So far, there are few reports on this aspect. Pang et al.[10] investigated the dissociation kinetic behavior of methane hydrate using thermal method in a closed middle-sized reactor of 10 L and observed a dramatically reduced dissociation rate phenomenon — "buffered dissociation" due to the ice melting. Yang et al.[23] developed a cylindrical reactor with an inner diameter of 300 mm and an effective height of 100 mm and investigated the gas production performance from
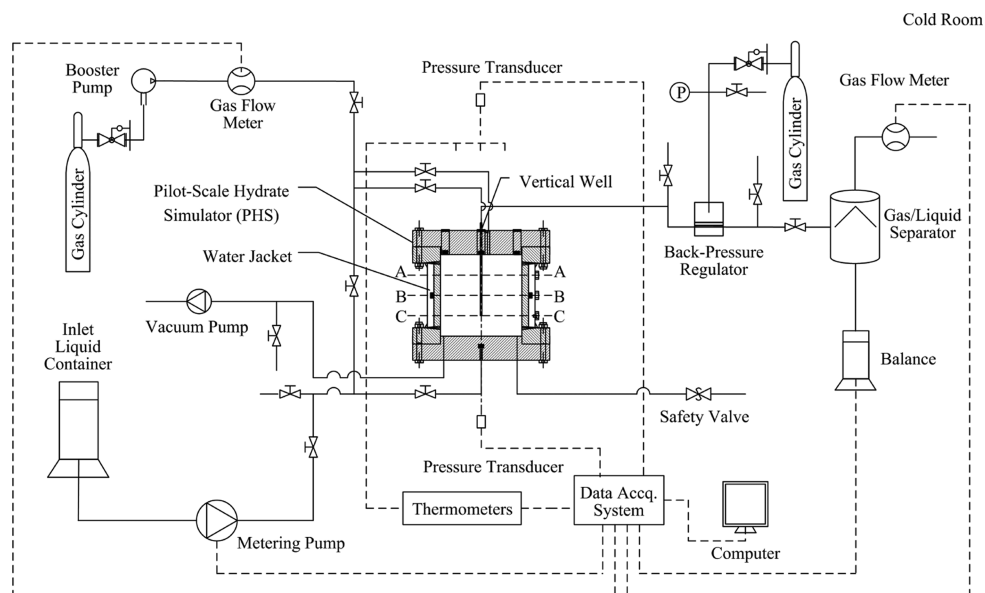
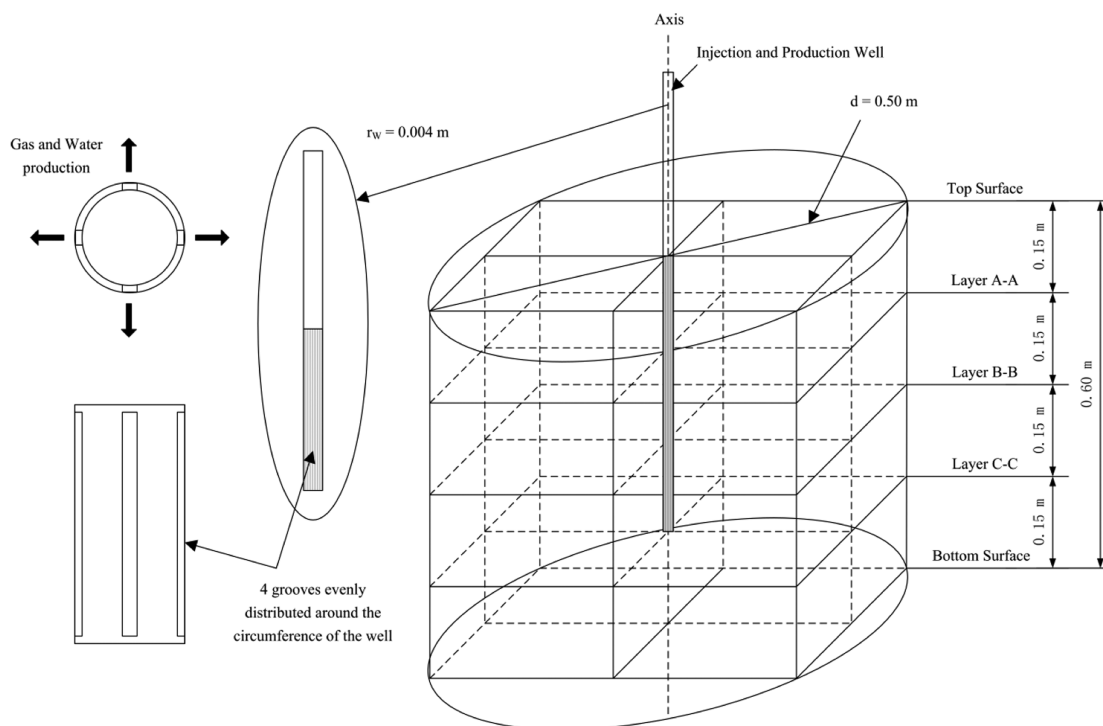**Figure 1.** Schematic of the experimental apparatus.

Figure 2. Schematic of the layers and the well design of the PHS.

methane hydrate. Recently, we have reported the investigation into the gas production behavior in a 3D cubic hydrate simulator (CHS) with the effective volume of 5.8 L. Both the depressurization[24] and huff and puff[25,26] methods have been employed to study the dissociation kinetic characteristics of methane hydrate in porous sediments. In addition, a pilot-scale hydrate simulator (PHS) with the effective volume of 117.8 L has been developed for hydrate formation and dissociation experiments, and some experimental results have been obtained using the huff and puff method.[18]

As another effective way of predicting the dynamic properties of hydrate dissociation in porous media, numerical simulation has been developing quickly in recent years. There have been various numerical codes developed for modeling nonisothermal hydration reactions in multiphase multicomponent systems. The TOUGH+HYDRATE (T+H) simulator is developed from TOUGH2 family codes at the Lawrence Berkeley National Laboratory. As one of the typical and representative codes, the T+H has been widely used to simulate the hydrate formation and decomposition under conditions typical of common natural CH_4-hydrate deposits (i.e., in the permafrost and in deep ocean sediments) in complex geological media at any scale (from laboratory to reservoir).[27] Li et al. used this code to evaluate the gas production potential from marine hydrate deposits in the Shenhu Area of South China Sea[21] and permafrost hydrate deposits in Qilian Mountain[22] with a single horizontal well by
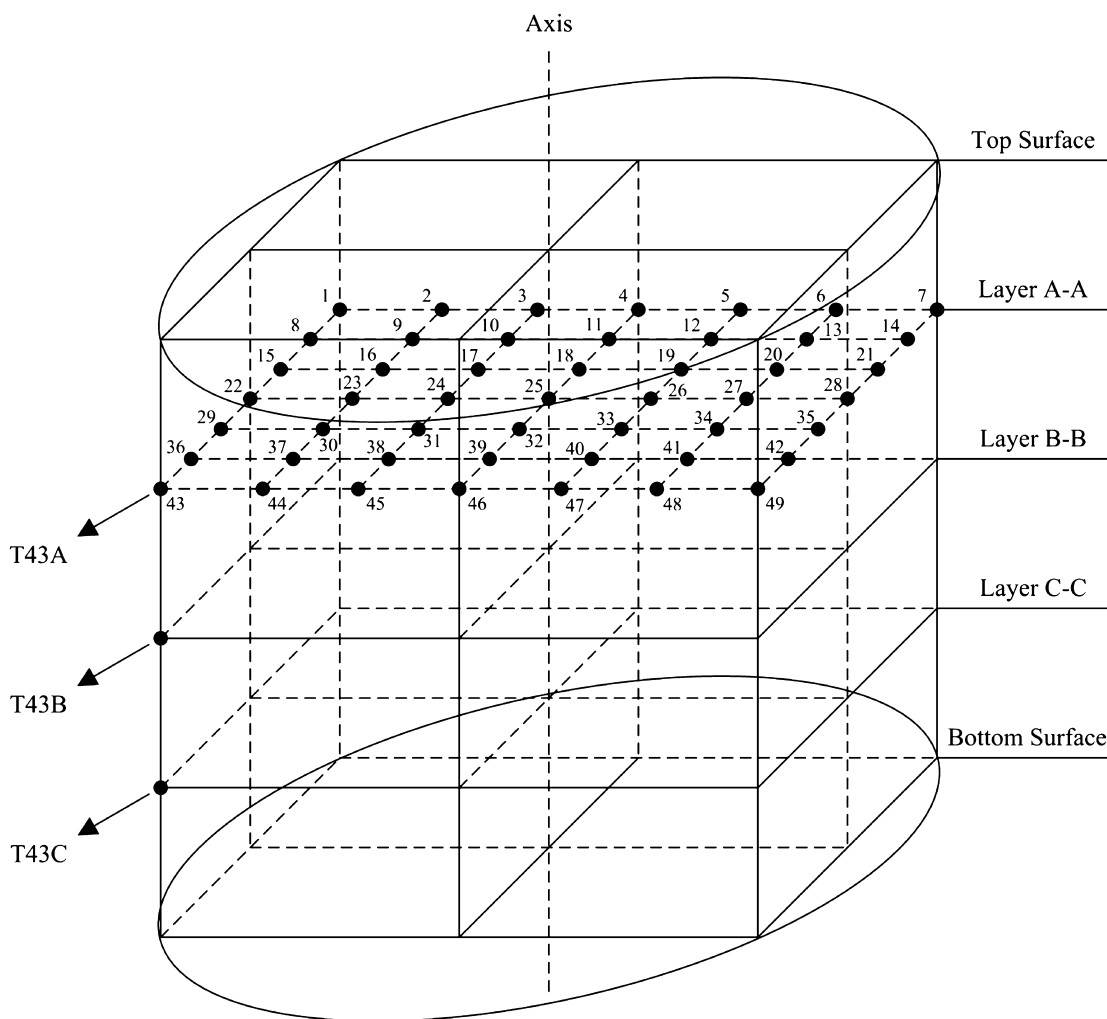
Figure 3. Schematic of the distribution of the thermometers in the PHS.

the huff and puff method. The results showed that the gas production was low from these hydrate deposits, but desirable gas-to-water ratio and energy efficiency could be obtained under suitable injection and production conditions in the Qilian Mountain permafrost hydrate deposits.

So far, the hydrate dissociation experiments in the PHS using the huff and puff method have been successfully carried out, but the corresponding numerical simulation has not yet been completed. In this work, we carried out both the experimental and numerical simulations to investigate the gas production behavior of methane hydrate in porous media using the huff and puff method in the PHS. The T+H simulator was chosen for numerical modeling. The mathematical and numerical models of the T+H code were validated by comparing the numerical and experimental results. A vertical well at the axis of the PHS was used as the injection and production well during the huff and puff process.

2. EXPERIMENT

2.1. Apparatus and Well Design. Figure 1 shows the schematic of the experimental apparatus used in this study, and a detailed description of the system is referred to in the published literature.[18,28] The PHS is a cylindrical stainless steel that can withstand pressures of up to 30 MPa. The effective volume of the PHS is 117.8 L (0.60 m length and 0.50 m diameter). The PHS is surrounded by a water jacket (−15−30 °C, ±0.1 °C), and the whole apparatus is placed in a walk-in

cold room (−8−30 °C, ±2 °C), which can provide the low-temperature conditions necessary for hydrate formation. Figure 2 shows the schematic of the layers and the well design of the PHS. As shown in Figures 1 and 2, the PHS is divided equally into four regions by three horizontal layers inside the vessel: the Layers A−A, B−B, and C−C. Each region has a height of 0.15 m. The central vertical well, with the radius of r_W = 0.004 m, is fixed at the axis of the PHS and extends into the vessel to the Layer C−C. It is used as the injection and production well during the huff and puff experiment.

As shown in Figure 2, there are four grooves evenly distributed along the circumference of the vertical well, and the grooves extend from the Top Surface of the PHS to the Layer C−C. Both the injected hot water and the produced fluid flow from these grooves. Previous studies have proposed two kinds of well design in gas production: (1) a single well with hot water injection and gas production simultaneously[29,30] and (2) a single well with hot water circulating inside the wellbore without coming in contact with the hydrate deposits.[31] Comparing with them, this kind of well design is much simpler and technologically feasible. Previous numerical studies have demonstrated the effectiveness of a similar grooved well design in gas production from marine and permafrost hydrate deposits.[21,22] Figure 3 shows the schematic of the distribution of the thermometers (the temperature measuring spots) in the PHS. There are a total of 147 thermometers evenly distributed in the PHS, with 49 spots on each layer (Layers A−A, B−B, and C−C). T25 is located at the center, and T1, T7, T43, and T49 are placed at the corner close to the cylindrical boundary. With the temperature records of these thermometers, we

can obtain the profiles of the evolution of the spatial distribution of T during the experiment.

The system pressure is measured with two pressure transducers. The "Inlet Pressure" transducer is located at the bottom of the PHS to measure the pressure of the base of the hydrate deposit, and the "Outlet Pressure" transducer is situated in the production well (the outlet of the well). A back-pressure regulator is connected to the outlet of the PHS to control the pressure of the production well. The cumulative gas injected into the PHS, the gas production rate, and the cumulative gas produced from the vessel are measured with two gas flow meters, which are situated in the inlet and outlet of the PHS, respectively. A balance is used to measure the mass of the produced liquid from the PHS. The performance and operation parameters of these transducers and devices as well as other related apparatus shown in Figure 1 are described in detail in the published literature.[18,28]

2.2. Experimental Procedure. The raw dry quartz sand with a size range between 300 and 450 μm was tightly packed in the PHS. The whole experiment consists of two stages: the hydrate formation stage and the dissociation stage. Figure 4 shows the evolutions of the
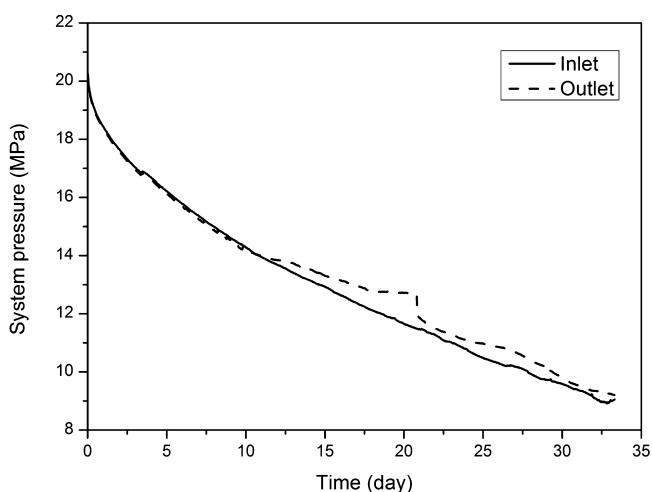

Figure 4. Evolutions of the Inlet and Outlet pressure during the hydrate formation.

Inlet and Outlet pressure during the hydrate formation stage. At the beginning of the hydrate formation process, the vessel was pressurized to approximately 20 MPa with methane gas and deionized water injection. The initial pore volume saturations of gas and water are 0.341 and 0.659, respectively. The total volume of gas before formation is 17.51 L (4,369 L in standard state). Then the vessel was closed as an isochoric system. After that, the temperature of the water jacket was gradually reduced to 7.3 °C as the hydrate formation equilibrium temperature. Using the fugacity model of Li et al.,[32] the equilibrium hydrate dissociation pressure at the working temperature was calculated to be about 5.3 MPa, which was much lower than the initial system pressure. The hydrate formation stage lasted for about 33 days, and the pressure of the vessel gradually decreased to 9.0 MPa. As shown in Figure 4, the descent speed of the Inlet and Outlet pressure declined due to the decreased driving force after this formation stage, so the hydrate formation experiment was halted at t = 33 days. The difference between the Inlet and the Outlet pressure during the late formation stage indicates that the solid hydrate may obstruct the gas diffusion in the PHS.

Then the following procedure was carried out to investigate into the dissociation behavior of methane hydrate using the huff and puff method. First, the pressure of the production well was gradually decreased to 5.53 MPa, which is slightly higher than the equilibrium pressure of 5.3 MPa. Gas was released from the vessel under the pressure driving force. Second, the vessel was closed for about 30 min, and the system pressure and temperature maintained stable, which indicated little hydrate dissociation during this period. After that, the

experimental and numerical simulation began (t = 0), and the huff and puff process was carried out for hydrate dissociation. The initial pressure and temperature of the vessel before hot water injection were 5.53 MPa and 7.18 °C, respectively. Each huff and puff cycle consisted of the following three stages: injection, soaking, and production. During the injection stage, hot water was injected into the vessel through the central vertical well to heat the deposit. The initial temperature of the injected hot water T_{inj} at the inlet of the well was about 85 °C, and it maintained stable. The injection rate Q_{inj} and the duration of the hot water injection t_{inj} maintained 0.2 L/min and 20 min, respectively. In the soaking stage, the injection well was closed for 30 min to allow the heat diffusion in the deposit. Then, during the production stage, the released gas and water were produced through the well by setting the back-pressure regulator pressure to 4.7 MPa. Once the system pressure declined to 4.7 MPa, the next huff and puff cycle began. This process was repeated until the system pressure stopped rising in the soaking stage. A total of 15 huff and puff cycles were carried out during the experiment. During the hydrate dissociation, the temperatures and pressures in the vessel, the water production rate, the gas production rate, and the cumulative gas produced were recorded by the data acquisition system at 20 s intervals.

3. NUMERICAL SIMULATION

3.1. The Numerical Simulation Code. In the numerical simulation study, we used both the serial and parallel versions of the TOUGH+HYDRATE code.[27,33] This code can model nonisothermal hydration reactions, phase behavior, and flow of fluids and heat under the conditions typical of natural CH_4-hydrate deposits in complex geologic media. The model accounts for heat and four mass components (i.e., water, CH_4, hydrate, and water-soluble inhibitors such as salts or alcohols) that are partitioned among four possible phases: gas, aqueous liquid, ice, and hydrate. A total of 15 states (phase combinations) can be described by the code, which can handle any combination of hydrate dissociation mechanisms. In this code, the impact of the movement and the volume expansion of the sediments are neglected.

3.2. System Properties and Domain Discretization. The system properties and parameters used in this simulation are shown in Table 1. The intrinsic permeability k (3.0 Darcies) and the wettability properties as well as other related parameters of the system are estimated based on the properties of quartz sand, of which the size range is 300−450 μm.

Figure 5 shows the simulation grid of the PHS. Because of axial symmetry, the cylindrical PHS is discretized into a radially symmetric mesh. It consists of 47 × 102 = 4,794 elements in (r, z), of which 4,601 are active (the remaining being boundary cells). The discretization along the r-axis is nonuniform, and it is discretized into 46 gridblocks within the PHS ($0 < r \leq 0.25$ m). The thickness of the gridblocks Δr increases from 0.002 to 0.007 m. The PHS is discretized into 100 gridblocks uniformly along the z-axis (-0.3 m $< z < 0.3$ m) with the thickness of Δz = 0.006 m. The uppermost ($z > 0.30$ m) and lowermost ($z <$ -0.30 m) layers are the top and bottom boundaries with the thickness of Δz = 0.007 m. The gridblocks of $r > 0.25$ m correspond to the cylindrical boundaries of the PHS, and their thickness is Δr = 0.007 m. All the boundary elements are impermeable and inactive during the simulation process, which means no fluids flow and constant pressure and temperature conditions. Assuming an equilibrium reaction of hydrate dissociation without inhibitors, this grid results in 14,382 coupled equations to be solved simultaneously.

Based on the well design of the experiment, a string of gridblocks with the radius of r_W = 0.004 m from the top surface

Table 1. Hydrate Deposit Properties and Conditions in the PHS

parameter	value
height of the PHS h	0.60 m
diameter of the PHS d	0.50 m
volume of the PHS V	117.8 L
initial pressure P_0	5.53 MPa
initial temperature T_0	280.63 K (7.48 °C)
density of the quartz sand	2600 kg/m³
gas composition	100% CH_4
initial saturations in the PHS	$S_H = 0.292$, $S_G = 0.326$, $S_A = 0.382$
intrinsic permeability $k_r = k_z$	3.0×10^{-12} m²(= 3.0 D)
porosity ϕ	0.435
water salinity	0
wet thermal conductivity $k_{\Theta RW}$	3.1 W/(m·K)
dry thermal conductivity $k_{\Theta RD}$	1.0 W/(m·K)
composite thermal conductivity model[27,37]	$k_{\Theta C} = k_{\Theta RD} + (S_A^{1/2} + S_H^{1/2})(k_{\Theta RW} - k_{\Theta RD}) + \varphi S_I k_{\Theta I}$
capillary pressure model[38]	$P_{cap} = -P_{01}\left[(S^*)^{-1/\lambda} - 1\right]^{1-\lambda}$ $S^* = (S_A - S_{irA})/(S_{mxA} - S_{irA})$
S_{irA}	0.04
λ	0.45
P_{01}	10^5 Pa
relative permeability model[27]	$k_{rA} = (S_A^*)^n$ $k_{rG} = (S_G^*)^{nG}$ $S_A^* = (S_A - S_{irA})/(1 - S_{irA})$ $S_G^* = (S_G - S_{irG})/(1 - S_{irA})$
n	3.572
n_G	3.572
S_{irG}	0.23
S_{irA}	0.10

to the Layer C−C are set to be the injection and production wells at the axis of the PHS, as shown in Figure 5. To avoid a theoretically correct but computationally intensive solution of the Navier−Stokes equation,[34] these wells are simulated as pseudoporous media with $\phi = 1.0$, $k = 3.0 \times 10^{-9}$ m² (3000 Darcies), and a capillary pressure $P_{cap} = 0$.

3.3. Initial and Boundary Conditions. At the beginning of the huff and puff process ($t = 0$), the domain of the PHS is saturated with three phases: hydrate, gas, and water. Based on the experimental results, the initial S_H, S_G, and S_A before hot water injection are calculated to be 0.292, 0.326, and 0.382, respectively, as shown in Table 1. According to the experimental results, the initial pressure P_0 is set to be 5.53 MPa, and the initial temperature T_0 is computed by the T+H internally to be 280.63 K (7.48 °C) with the equilibrium model of methane gas. It is in accordance with the experimental value of 280.33 K (7.18 °C, the average of the 147 thermometers), which indicates the accuracy of the P-T equilibrium model of the T+H code. Thus the initial values of the primary variables (P, S_A, and T) of each grid have been determined.

Figure 6 shows the profile of the boundary temperature T_B of the experimental results during hydrate dissociation in the PHS. It shows the characteristics in each huff and puff cycle that the temperature of the stainless steel boundary rises continuously during the hot water injection stage and the soaking stage, while it drops down sharply in the production stage. This is caused by the heat conduction between the boundary and the deposit during the huff and puff process. The boundary temperature of the numerical simulation process is based on the experimental results shown in Figure 6.
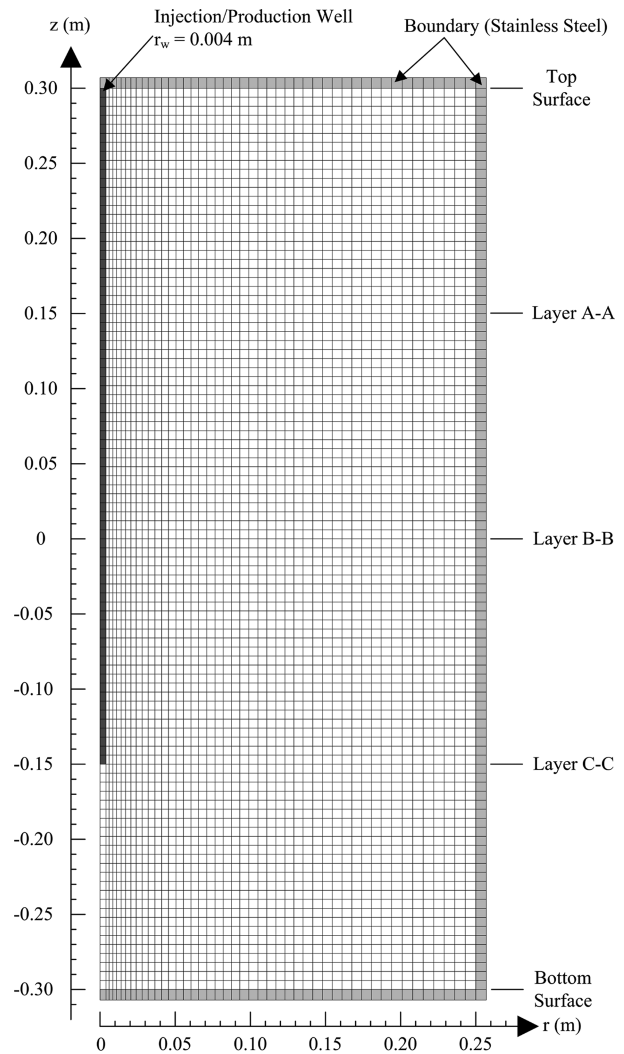

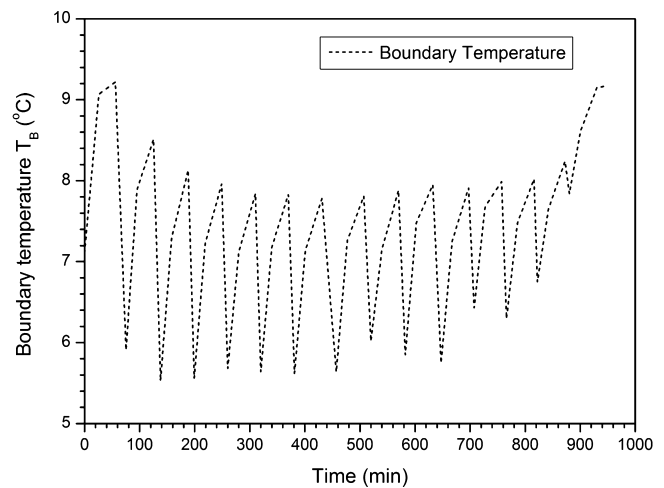**Figure 5.** Schematic of the grid used in the numerical simulation.

Figure 6. Boundary temperature T_B profile of the experimental results during hydrate dissociation in the PHS.

3.4. Simulation Procedure. Based on the experimental results, the numerical simulation course consists of 15 huff and puff cycles. Each cycle is divided into three stages (injection, soaking, and production) to simulate separately. For example, at the beginning of the injection stage of the first cycle ($t = 0$),

the hot water is injected into the PHS with constant rate of Q_{inj} = 0.2 L/min for 20 min through the injection well, as shown in Figure 5. When the injection stage is over, the soaking starts immediately, and the mass injection and production rates of the well are set to be 0. After 30 min of soaking, the production stage starts and lasts for about 19.33 min, which is the duration of the production stage of the first cycle in the experiment simulation. During this stage, the well performs as a sink term, and the constant mass production rate Q_{pro} is determined through a trial-and-error simulation process that results in the known system pressure of P = 4.7 MPa at the end of the production stage. When the first cycle ends, the second cycle begins with similar operation conditions and so on. According to the experiment, the temperature and the salinity of the injected hot water maintain T_{inj} = 85 °C and X_S = 0, respectively.

4. RESULTS AND DISCUSSION

4.1. Pressure Profiles and Spatial Distribution. Figure 7 shows the comparison of the experimental and numerical
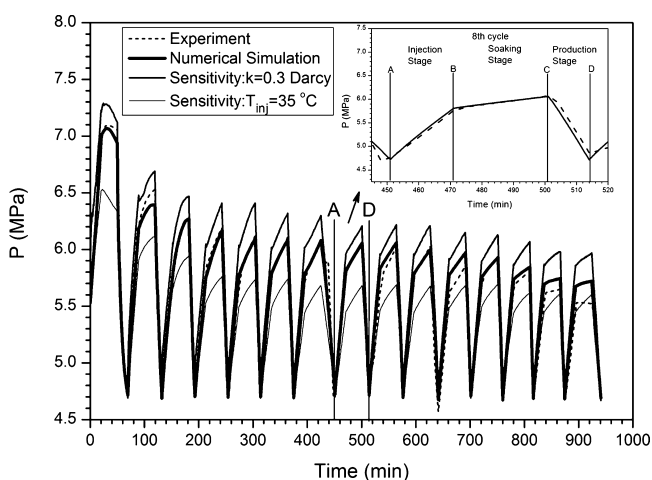

Figure 7. Comparison of the experimental and numerical simulation results of the system pressure P during hydrate dissociation in the PHS and its sensitivities to k and T_{inj} of the numerical simulation.

simulation results of the system pressure P over time during hydrate dissociation in the PHS. Both the experimental and numerical simulation results show a regular fluctuation of the system pressure during the huff and puff process. As a typical example, the pressure evolution with time of the eighth cycle is shown in the partial enlarged plot of Figure 7. It starts at t = 451 min (Point A) and ends at t = 514 min (Point D). In the hot water injection stage of 451−471 min (A−B), the system pressure increases continuously to approximately 5.80 MPa, which is caused by (i) the mass injection, (ii) the released gas from hydrate dissociation under thermal stimulation, and (iii) the thermal expansion effect of methane gas under high temperature conditions. Within the soaking stage of 471−501 min (B−C), the system pressure continues increasing when the injected heat diffuses from the well to the deposit to promote more hydrate dissociation. However, the increment speed in the soaking stage is much lower than that in the injection stage, which indicates a limited hydrate dissociation rate caused by the decreased heat conduction efficiency in this period. During the production stage of 501−514 min (C−D), the PHS is depressurized sharply from about 6.07 to 4.70 MPa, and both

gas and water are produced from the vessel through the production well. The fluctuation range of the pressure nearly keeps the same in each cycle except the first one, which is because the first cycle starts at P = 5.53 MPa, while the others begin at P = 4.70 MPa. It also shows that the maximum pressure of each cycle gradually declines due to the decreased hydrate dissociation rate.

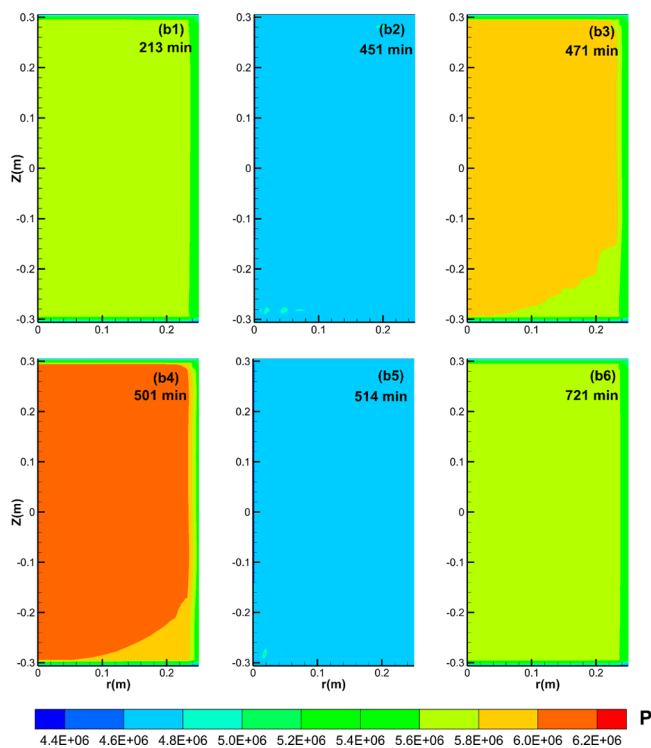Figure 8 shows the numerical simulation results of evolution of the P spatial distribution during hydrate

Figure 8. Evolution of the spatial distribution of P during hydrate dissociation in the PHS.

dissociation in the PHS. In this study, the figures marked with "a" represent the experimental results, while those with "b" represent the corresponding numerical simulation results. The time points of figures b1 and b6 are the end of the injection stage of the fourth and the 12th huff and puff cycles, respectively, and figures b2−b5 correspond to the four time points of A−D in the eighth cycle shown in the enlarged plot of Figure 7, respectively. We can see that the pressures at different locations in the PHS have little discrepancy because of the high porosity and permeability of the sediment, which validates the experimental assumption that the pressure at any point of the PHS can be taken as the system pressure, including the pressures measured by the Inlet and Outlet Pressure transducers used in the experiment. The pressure at each time point in Figure 8 is in accordance with that shown in Figure 7. Figure 8(b1, b3, and b6) shows that the system pressure increases approximately to the same level at the end of each injection stage, which means the pressure fluctuation in this stage is mainly controlled by the amount of the injected hot water. Comparing Figure 8(b2) with Figure 8(b5), we can see that the pressure decreases exactly to 4.70 MPa at the end of each production stage. During a single huff and puff cycle, the pressure increases to the maximum at the end of the soaking stage, as shown in Figure 8(b4).

4.2. Gas and Water Production. Figures 9 and 10 show the comparisons of the experimental and numerical simulation
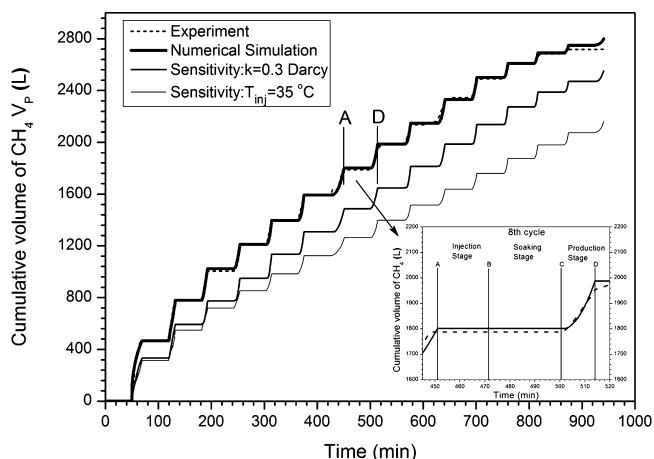

Figure 9. Comparison of the experimental and numerical simulation results of the cumulative gas produced V_P during hydrate dissociation in the PHS and its sensitivities to k and T_{inj} of the numerical simulation.
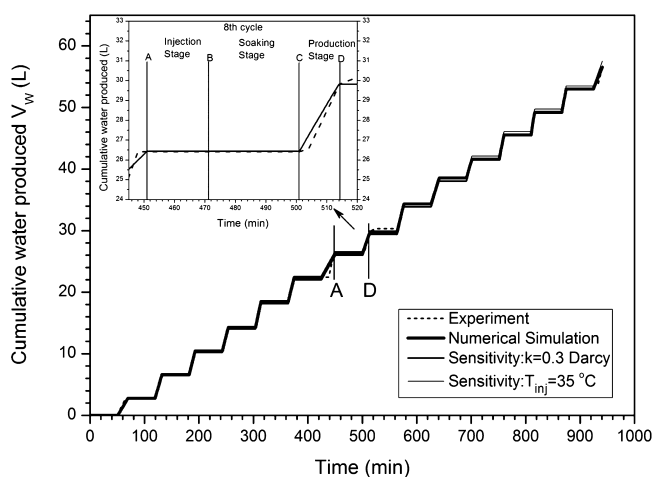

Figure 10. Comparison of the experimental and numerical simulation results of the cumulative water produced V_W during hydrate dissociation in the PHS and its sensitivities to k and T_{inj} of the numerical simulation.

results of the cumulative volume of the produced gas (V_P) and water (V_W) during the hydrate dissociation in the PHS. Both of them increase with time in the form of ladder. As a typical example, the gas and water production of the eighth cycle (A−D) are also shown in the partial enlarged plots of Figures 9 and 10, respectively. Hot water is injected into the vessel in the injection stage (A−B) with constant rate $Q_{inj} = 0.2$ L/min for 20 min, and the amount of the injected mass is 4.0 kg. When the well is closed, there is no fluid injection or production in the soaking stage (B−C). Both of the V_P and V_W maintain constant in 451−501 min (A−C). When the production stage starts, gas and water are produced from the vessel continuously. The cumulative volume of the produced gas and water of the numerical simulation during this production stage (C−D) are about 186 and 3.38 L, respectively, while they are 167 and 3.40 L, respectively, in the experiment. The numerical results agree well with the experiment, which indicates the accuracy of the fluids flow model used in this study.

As shown in Figure 9, the volume of the produced CH_4 in the first cycle is relatively higher than the others. This is because the PHS is depressurized from about 7.06 to 4.70 MPa in the first production stage, while others are from less than 6.50 MPa (Figure 7). In addition, the gas production rate maintains approximately stable in a relatively long period (second−11th cycles), which indicates a steady heat absorption and hydrate dissociation process. In the later production stage (12th−15th cycles), the cumulative gas produced in each cycle gradually decreases over time because the hydrate dissociation rate decreases when the heat conduction efficiency reduces with the expansion of the dissociation area. The average gas production rate Q_{avg} is about 2.89 L/min in the end. During the entire huff and puff process (0−941 min), the water is produced from the vessel with an average rate of about 3.8 L/cycle, and the difference of the water production between each cycle is very slight. However, this average water production rate is lower than the hot water injection rate (4.0 L/cycle) in each cycle, which indicates that some of the injected water is retained in the vessel. So the water production is manageable when using the huff and puff method for hydrate dissociation. Similar results of the gas and water production behaviors using the huff and puff method have been concluded in previous studies.[18,22,26]

Figure 11 shows the comparison of the experimental and numerical simulation results of the gas-to-water ratio $R_{GW} =$
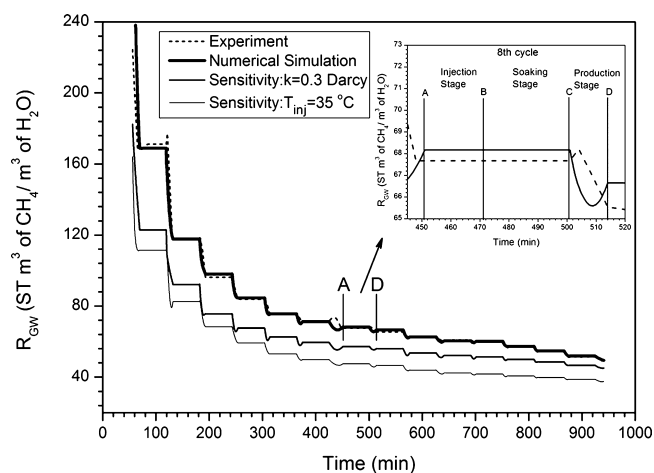

Figure 11. Comparison of the experimental and numerical simulation results of the gas-to-water ratio R_{GW} during hydrate dissociation in the PHS and its sensitivities to k and T_{inj} of the numerical simulation.

V_P/V_W during hydrate dissociation in the PHS. R_{GW} is a relative criterion of gas production performance and can measure the effectiveness of hydrate dissociation as a gas-producing method. It is shown that R_{GW} declines quickly to approximately 75.5 ST m^3 of CH_4/m^3 of H_2O after the first 5 huff and puff cycles (0−314 min). After that, the descent speed slows down because of the relatively stable gas and water production rate in this period (Figures 9 and 10). At the end of the experiment, R_{GW} declines to the minimum of about 49.5. As shown in the partial enlarged plot of Figure 11, the R_{GW} maintains stable during the injection and soaking stages, and it rises slightly in the early production stage in the experiment. It may be because some of the released methane gas gradually accumulates at the top of the vessel because of buoyancy during the soaking stage, and it further results in a higher gas production rate and a lower water

production rate in the early production stage (as shown in Figures 9 and 10).

Figure 12 shows the comparison of the experimental and numerical simulation results of the energy efficiency η during
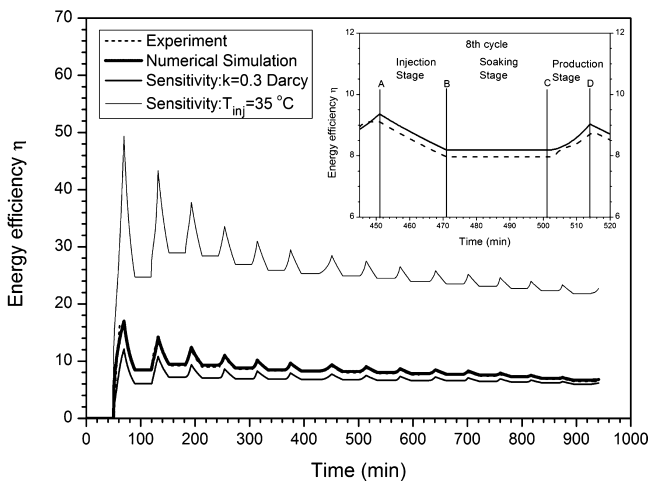

Figure 12. Comparison of the experimental and numerical simulation results of the energy efficiency η during hydrate dissociation in the PHS and its sensitivities to k and T_{inj} of the numerical simulation.

hydrate dissociation in the PHS. It is defined as the ratio of the amount of energy produced in the form of CH_4 to the energy provided to the reservoir,[22] as shown in the following equation

$$\eta = \Delta H_c / (W + Q)$$

where ΔH_c is the total enthalpy of combustion of CH_4 (1 atm, 25 °C, 889.6 kJ/mol), W is the pressurization energy consumed by the pump,[22] and Q is the heat used for heating the injected water. It is assumed that the water is heated from 20 °C to the injection temperature T_{inj}. It is shown in the partial enlarged plot of Figure 12 that η increases in the production stage (C−D), while it drops down in the injection stage when the heat and the pressurization energy is consumed by the system. During the whole huff and puff process, η gradually decreases from the maximum of about 16.5 to the minimum of about 6.5 in the Reference Case.

4.3. Spatial Distribution of T. Figure 13 shows the comparison of the evolutions of the T spatial distributions over time of the experimental and numerical simulation results during hydrate dissociation using the huff and puff method in the PHS. Figures 13(a1)−(a6) are the experimental temperature results that are obtained by the 147 thermometers distributed in the three layers shown in Figure 3. The numerical results of the T distribution over time are shown in Figures 13(b1)−(b6), and because of axial symmetry, only a cross-section of the PHS is plotted. The temperature measuring spots in Figures 13(a1), (b1), and (b2) are in accordance with the distributions of the thermometers shown in Figure 3. The time points of Figures 13(a1)−(a6) and (b1)−(b6) are the same as those mentioned in Figure 8. The solid rectangle formed by T25A, T25C, T28C, and T28A in Figure 13(b1) corresponds to that in Figure 13(a1). The dashed rectangle of T25A, T25C, T7C, and T7A in Figure 13(b2) corresponds to that in Figure 13(a1).

Generally, the numerical results of the T distribution at each time point show fine agreements with the experiment, which indicates the accuracy of the heat transfer model used in this
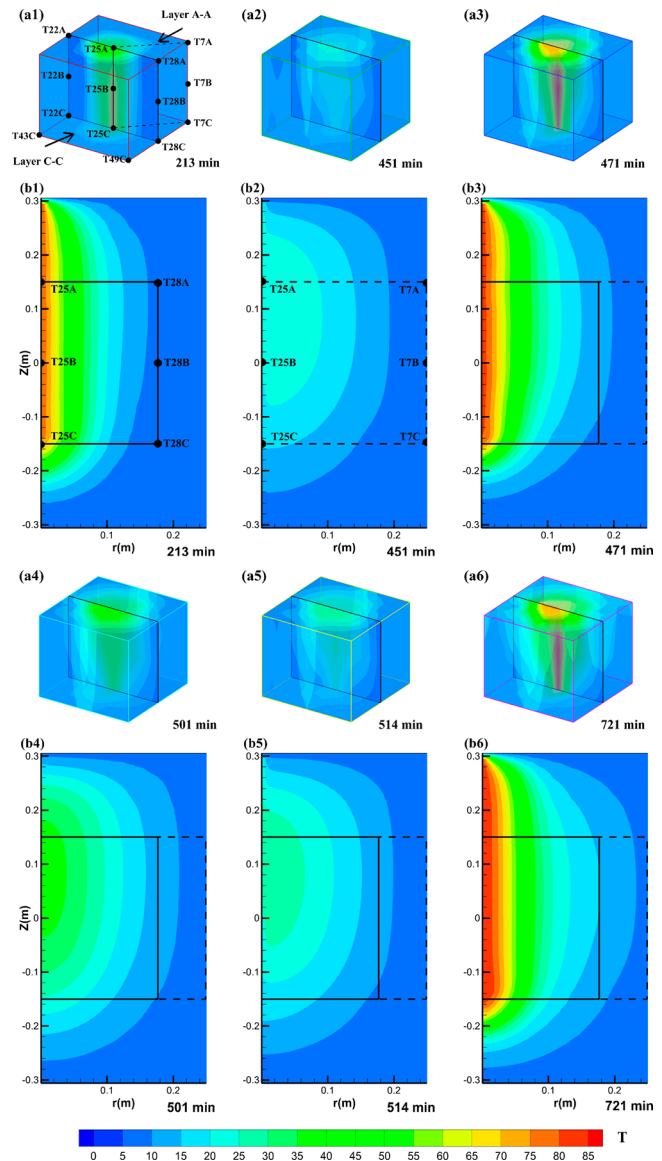

Figure 13. Comparison of spatial distributions of T over time of experimental (a1−a6) and numerical simulation (b1−b6) results during hydrate dissociation in the PHS.

study. Both of the experimental and numerical results show the following characteristics during the injection stage: (i) the highest temperature ($T > 80$ °C) in the PHS is observed in the vicinity of the injection well, and the high-T region gradually enlarges in different injection stages, indicating more heat absorbed by the quartz sand and the external surroundings during the huff and puff process; (ii) the injected hot water has an approximately cylindrical moving front around the well. With the constant injection rate $Q_{inj} = 0.2$ L/min ($t_{inj} = 20$ min) and assuming that the hot water flows from the well to the inner deposit of the PHS along the r-axis, the calculated radius of the hot water moving front at the end of the injection stage during each huff and puff cycle is approximately $r = 0.08$ m, which is about in the region of $T > 35$ °C, as shown in Figures 13(b1), (b3), and (b6). It is much smaller than the thermal effect range (defined as the area of $T > 10$ °C) within which the hydrate is thought to be completely dissociated, so the conduction performs as the main heat transfer pattern in the PHS, which is coincident with the results of previous

studies.[21,22] The thermal effect range gradually enlarges with the huff and puff process going on, as shown in Figures 13(a1), (a3), and (a6).

During the soaking step, one part of the injected heat is conducted to the inner deposit to dissociate the methane hydrate, while another part diffuses to the area far away from the well to be absorbed by the quartz sand and the outside surroundings through the boundary, resulting in the temperature decrease around the well (Figures 13(a4) and (b4)). It can be seen from Figures 13(a5) and (b5) that the temperatures in the vessel decline obviously during the production stage, and the thermal effect range shrinks due to (i) the endothermic reaction of the hydrate dissociation under depressurization and (ii) the cooling effect of the cold fluid flow from the undissociated zone in the vicinity of the boundary to the well. The temperature decreases to lower than 30 °C at the end of the eighth huff and puff cycle (Figure 13(b5)).

4.4. Hydrate Dissociation Rate and Spatial Distribution of S_H. Figure 14 shows the comparison of the
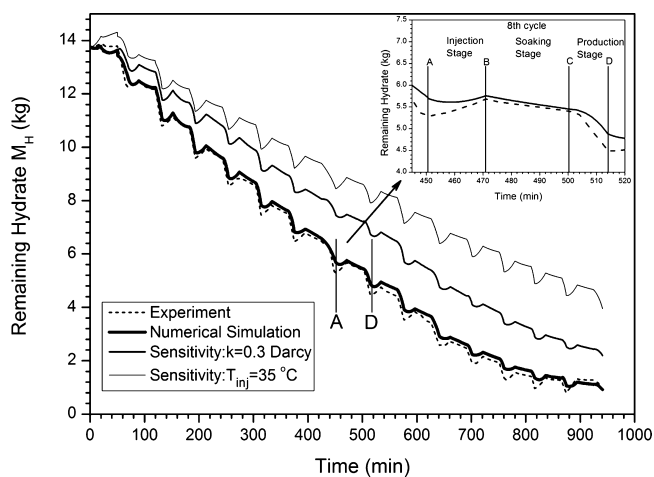

Figure 14. Comparison of the experimental and numerical simulation results of the remaining undissociated hydrate M_H over time in the PHS and its sensitivities to k and T_{inj} of the numerical simulation.

experimental and numerical simulation results of the remaining undissociated hydrate M_H over time in the PHS. In order to calculate the remaining mass of the three phases (gas, water, and hydrate) in the vessel, we assume that the water and the sand grains are incompressible, and the effective pore volume in the PHS do not change during the whole experiment. Then the mass of the remaining hydrate with time in the PHS is determined through the temperature and pressure measurements and the mass balance calculations using the Peng–Robinson equation.[35] The initial mass of the hydrate in the PHS is about 13.6 kg for both of the experiment and the numerical simulation.

As shown in Figure 14, both the experimental and numerical simulation results indicate that the hydrate in the PHS is dissociated gradually during the entire production process and secondary hydrate formation exists in each huff and puff cycle in the injection stage. As a typical example, the remaining hydrate of the eighth cycle (A−D) is shown in the partial enlarged plot of Figure 14. After the hot water is injected into the PHS from the central vertical well, the gas and water in the vicinity of the well are gradually driven from the well to the inner deposit, resulting in the increase of the system

pressure, which has already been discussed in Figure 7. As the temperature in the area adjacent to the boundary is lower than that in the thermal effect range discussed above (Figure 13), the secondary hydrate begins to form when the pressure increases to be higher than the equilibrium pressure under the mass injection, resulting in an increase of the hydrate in the PHS shown in Figure 14. After ceasing the hot water injection stage, the dissociation process is dominant, and there is gas releasing from hydrate dissociation. During the production stage of the eighth cycle (C−D), the hydrate dissociation rate becomes faster under the depressurization effect, and the total mass of the dissociated hydrate in the production stage is more than that in the soaking stage, which implies that depressurization rather than thermal stimulation is dominant for the hydrate dissociation.[18] The diminishing downtrend of the remaining hydrate indicates that the hydrate dissociation rate decreases over time. This is because the injected water is restricted in the vicinity of the well, and the conduction as the main heat transfer pattern in the PHS has very limited efficiency. After 15 huff and puff cycles, the remaining hydrate is about 0.92 kg, which means that 93.3% of the hydrate has been dissociated.

Figure 15 shows the evolution of the spatial distribution of S_H over time during the hydrate dissociation. The selected three time points are the end of the injection stages of the fourth, the eighth, and the 12th huff and puff cycles, respectively. Generally, the whole PHS is divided into the hydrate dissociated zone and the undissociated zone by an irregular dissociation interface, and this interface expands gradually toward the hydrate body away from the well, which confirms that the hydrate dissociation is an analog of a moving boundary ablation process.[36] As shown in Figure 15, the hydrate undissociated zone is in accordance with the low-T area shown in Figure 13. During the injection stage, when the released gas is driven away from the well toward the undissociated area (close to the top and bottom surfaces as well as the cylindrical boundary) by the injected water, secondary hydrate is formed under favorable pressure and temperature conditions in this area, and the hydrate saturation rises to about 0.40, which is much higher than the initial value of 0.292. On the other hand, the distributions in Figure 15 show that the remaining hydrate is mainly distributed in the area far away from the well, so the hydrate dissociation mainly occurs in this area where the injected hot water could not be involved in most of the huff and puff cycles. During the late huff and puff process, the dissociation interface near the cylindrical boundary gradually disappears, while that in the top and bottom corners of the PHS still exists after the entire production process. This is because they are far away from the injection well, and most of the injected heat is mainly transferred to the outside surroundings through the boundaries other than to the hydrate regions.

4.5. Sensitivity to k and T_{inj}. In this study, we investigate into the sensitivity of gas production to the intrinsic permeability k and the temperature of the injected hot water T_{inj} through numerical simulation. The case described above is regarded as the Reference Case. Figures 7, 9, 10, 11, 12, and 14 show, respectively, the dependences of P, V_P, V_W, R_{GW}, η, and M_H over time in the PHS on k and T_{inj}.

When the intrinsic permeability k is decreased from 3.0 to 0.3 Darcy, the well pressure increases to a higher level during the injection and soaking periods in each huff and puff cycle comparing with the Reference Case (Figure 7) when the effective permeabilities k_{eff} of gas and water are both decreased.
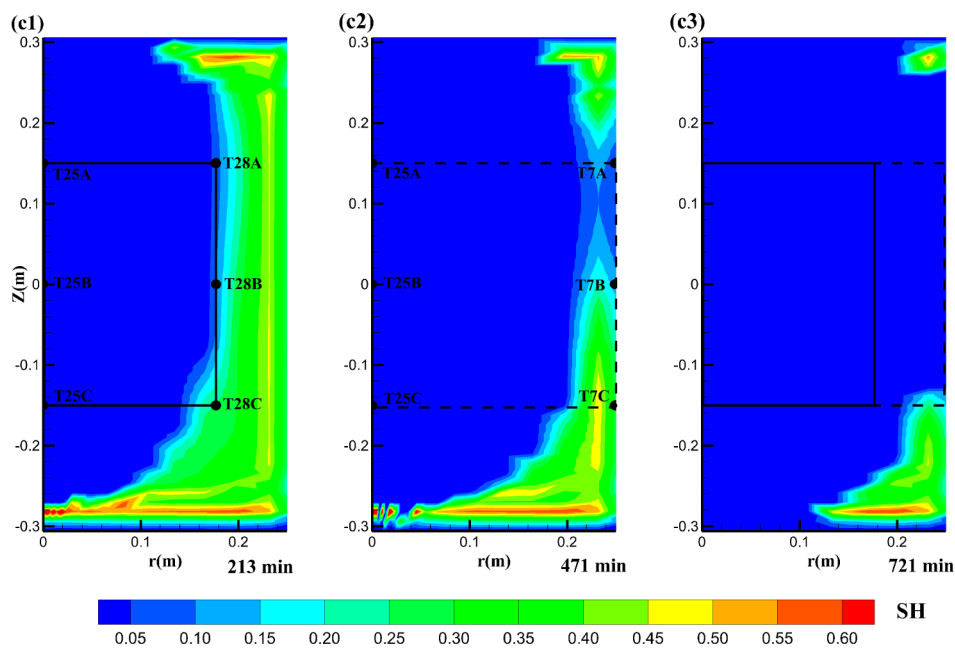
Figure 15. Numerical simulation results of the spatial distribution of S_H over time during hydrate dissociation in the PHS.

There is obvious decline of V_P with a decrease of k (Figure 9), while V_W (Figure 10) nearly keeps the same with the Reference Case, which means that the gas production performance is more favorable with a higher k and the water production is manageable using the huff and puff method. Meanwhile, both the gas-to-water ratio R_{GW} and the energy efficiency η decrease under the condition of $k = 0.3$ D, as shown in Figures 11 and 12. Besides, the hydrate dissociation rate slows down when the injected hot water could not soak into the inner deposit effectively due to the decreased k_{eff} (Figure 14). Generally, the gas production is favored by a high intrinsic permeability k of the hydrate deposit.

When the temperature of the injected water is reduced from 85 to 35 °C, the pressure rises to lower levels than the Reference Case during the injection and soaking stages (Figure 7). This is because there is less gas released from hydrate dissociation when the injected heat is decreased. In addition, there is obvious decline of V_P comparing with the Reference Case (Figure 9), which indicates that the lower the temperature of the injected hot water is, the less heat it can provide for hydrate dissociation in the injection stage and the less gas released from hydrate. However, the cumulative water produced in each cycle still remains nearly the same with the Reference Case and the case of $k = 0.3$ D (Figure 10). So the gas-to-water ratio is decreased from about 50.0 to 38.0 with the temperature decline of the injected water (Figure 11). Figure 12 shows that the energy efficiency increases by about 2.5 times under the condition of $T_{inj} = 35$ °C as the heat provided to the system is dramatically reduced. So a lower injection temperature will be more profitable, and it is not necessary to heat the water to an extremely high temperature level from this point of view. As shown in Figure 14, the hydrate dissociation rate is decreased obviously during the whole simulation period when the injection temperature is reduced to 35 °C, which proves that the injected heat plays an important role in the huff and puff hydrate dissociation process. On the other hand, the amount of secondary hydrate formed in the injection stage is more than that of the Reference Case, which is caused by the lower heat transfer rate from the injection well to the inner hydrate deposit.

5. CONCLUSIONS

In this work, we investigate by means of experimental and numerical simulation the gas production behavior of methane hydrate in porous media in the novel Pilot-Scale Hydrate Simulator (PHS). The huff and puff method is employed for hydrate dissociation in a single vertical well placed at the axis of the PHS. Each huff and puff cycle consists of three stages: the injection stage, the soaking stage, and the production stage. Based on the results of this study, the following conclusions are drawn from the experimental and numerical simulation.

In the Reference Case ($T_{inj} = 85$ °C, $Q_{inj} = 0.2$ L/min, $t_{inj} = 20$ min), both the experimental and numerical simulation results show a regular fluctuation of the system pressure during the huff and puff process, and the increment speed in the soaking stage is much lower than that in the injection stage. Because of the high porosity and permeability of the sediment, the pressures at different locations in the PHS have little discrepancy and any of them can be taken as the system pressure. With the constant hot water injection rate, it shows that the injected hot water has an approximately cylindrical moving front around the well, and it is mainly restricted in the area of $r < 0.08$ m. The conduction performs as the main heat transfer pattern in the PHS for hydrate dissociation. The highest temperature (more than 80 °C) is observed in the vicinity of the injection well at the end of the injection stage, and the high-T region gradually enlarges in different injection stages with more heat absorbed by the quartz sand and the external surroundings.

The gas production rate maintains approximately stable in a relatively long period, while it decreases over time with the decrease of the hydrate dissociation rate in the later production stage. As the absolute criterion of gas production performance, the average gas production rate Q_{avg} is about 2.89 L/min in the end. During the entire huff and puff process, the average water production rate is about 3.8 L/cycle, which is lower than the

hot water injection rate. The mass of the water produced in each cycle has little difference and is manageable when using the huff and puff method. The long-term gas-to-water ratio R_{GW} is more than 49.5 ST m^3 of CH$_4$/m^3 of H$_2$O, and the energy efficiency is about 6.5 at the end of the experiment, indicating the effectiveness and economic efficiency of the huff and puff method from the relative criterion point of view. The hydrate is dissociated gradually during the entire production process, and secondary hydrate formation exists in each huff and puff cycle in the injection stage.

The numerical analysis of sensitivity to k indicates that the deposit with higher intrinsic permeability will show better gas production performance as the flow conditions become more favorable for the released gas. A decrease of the intrinsic permeability will result in a declined hydrate dissociation rate when the hot water could not soak into the hydrate deposit effectively due to the decreased k_{eff}. Generally, a higher k is associated with higher gas production and more beneficial R_{GW} and η, while the water production rate changes little during the huff and puff process. In addition, the numerical analysis of sensitivity to T_{inj} indicates that the hydrate dissociation, the gas production rate, and the gas-to-water ratio can be enhanced by raising the temperature of the injected hot water, while it has little effect on the water production rate in each huff and puff cycle. However, higher T_{inj} will results in lower energy efficiency as more heat is needed for heating the injected water. Lower injection temperature may be more profitable using the huff and puff method.

The numerical simulation results of the pressure profiles, the gas and water production, the gas-to-water ratio, the energy efficiency, the spatial distribution of T, and the remaining hydrate in the PHS all agree well with the experiment, which demonstrates that the model can describe the hydrate formation and dissociation behaviors well in porous media during the huff and puff process. So it is concluded that our developed model can predict the gas production performance from complex porous media.

■ AUTHOR INFORMATION

Corresponding Author
*Phone/Fax: +86 20 87057037. E-mail: lixs@ms.giec.ac.cn.

Notes
The authors declare no competing financial interest.

■ ACKNOWLEDGMENTS

■ NOMENCLATURE

d = diameter of the PHS (m)
h = height of the PHS (m)
k = intrinsic permeability (m^2)
k_{eff} = effective permeability (m^2)
k_{rA} = aqueous relative permeability (m^2)
k_{rG} = gas relative permeability (m^2)
$k_{\Theta C}$ = thermal conductivity (W/(m·K))
$k_{\Theta RD}$ = thermal conductivity of dry porous medium (W/(m·K))

$k_{\Theta RW}$ = thermal conductivity of fully saturated porous medium (W/(m·K))
$k_{\Theta I}$ = thermal conductivity of ice (W/(m·K))
M_H = remaining hydrate mass (kg)
P = pressure (MPa)
Q_{avg} = average gas production rate (L/min)
Q_{inj} = hot water injection rate (L/min)
Q_{pro} = mass production rate (kg/s)
R_{GW} = cumulative gas to water production ratio (ST m^3 of CH$_4$/m^3 of H$_2$O)
S_A = initial aqueous saturation, volume
S_G = initial gas saturation, volume
S_H = initial hydrate saturation, volume
r = radius
r,z = cylindrical coordinates (m)
T = temperature (°C)
t = time (min)
t_{inj} = duration of the hot water injection (min)
T_{inj} = initial temperature of the hot water (°C)
V = volume of the PHS (L)
V_P = cumulative volume of the produced CH$_4$ (L)
V_W = cumulative volume of the produced water (L)
X_S = salinity
Δr = discretization along the r-axis (m)
Δz = discretization along the z-axis (m)
ϕ = porosity
λ = van Genuchten exponent - Table 1

Subscripts and Superscripts

0 = denotes initial state
A = aqueous phase
B = boundary
cap = capillary
G = gas phase
H = solid hydrate phase
I = ice phase
irA = irreducible aqueous phase
irG = irreducible gas
n = permeability reduction exponent - Table 1
n_G = gas permeability reduction exponent - Table 1
S = salinity
W = well

■ REFERENCES

(1) Sloan, E. D.; Koh, C. A. *Clathrate Hydrates of Natural Gases*, 3rd ed.; CRC Press: Boca Raton, FL, 2008.
(2) Collett, T. S. Gas hydrates as a future energy resource. *Geotimes* **2004**, *49* (11), 24−27.
(3) Moridis, G. J.; Silpngarmlert, S.; Reagan, M. T.; Collett, T.; Zhang, K. Gas production from a cold, stratigraphically-bounded gas hydrate deposit at the Mount Elbert Gas Hydrate Stratigraphic Test Well, Alaska North Slope: Implications of uncertainties. *Mar. Pet. Geol.* **2011**, *28* (2), 517−534.
(4) Li, G.; Moridis, G. J.; Zhang, K.; Li, X. S. Evaluation of gas production potential from marine gas hydrate deposits in Shenhu Area of South China Sea. *Energy Fuels* **2010**, *24*, 6018−6033.
(5) Ahmadi, G.; Ji, C. A.; Smith, D. H. Production of natural gas from methane hydrate by a constant downhole pressure well. *Energy Convers. Manage.* **2007**, *48* (7), 2053−2068.
(6) Moridis, G. J.; Reagan, M. T.; Boyle, K. L.; Zhang, K. Evaluation of the gas production potential of some particularly challenging types of oceanic hydrate deposits. *Transp. Porous Media* **2011**, *90* (1), 269−299.
(7) Tang, L. G.; Xiao, R.; Huang, C.; Feng, Z. P.; Fan, S. S. Experimental investigation of production behavior of gas hydrate

under thermal stimulation in unconsolidated sediment. *Energy Fuels* **2005**, *19* (6), 2402−2407.

(8) Li, G.; Li, X. S.; Tang, L. G.; Li, Q. P. Control Mechanisms for Methane Hydrate Production by Thermal Stimulation. In *The 6th International Conference on Gas Hydrate*; Vancouver, British Columbia, Canada, 2008; Paper 5783.

(9) Yang, X.; Sun, C. Y.; Yuan, Q.; Ma, P. C.; Chen, G. J. Experimental study on gas production from methane hydrate-bearing sand by hot-water cyclic injection. *Energy Fuels* **2010**, *24*, 5912−5920.

(10) Pang, W. X.; Xu, W. Y.; Sun, C. Y.; Zhang, C. L.; Chen, G. J. Methane hydrate dissociation experiment in a middle-sized quiescent reactor using thermal method. *Fuel* **2009**, *88* (3), 497−503.

(11) Li, D. L.; Liang, D. Q.; Fan, S. S.; Li, X. S.; Tang, L. G.; Huang, N. S. In situ hydrate dissociation using microwave heating: Preliminary study. *Energy Convers. Manage.* **2008**, *49* (8), 2207−2213.

(12) Kawamura, T.; Yamamoto, Y.; Ohtake, M.; Sakamoto, Y.; Komai, T.; Haneda, H. Experimental study on dissociation of hydrate core sample accelerated by thermodynamic inhibitors for gas recovery from natural gas hydrate. In *The 5th International Conference on Gas Hydrate*; Trondheim, Norway, 2005; pp 3023−3028.

(13) Li, G.; Li, X. S; Tang, L. G; Zhang, Y. Experimental investigation of production behavior of methane hydrate under ethylene glycol stimulation in unconsolidated sediment. *Energy Fuels* **2007**, *21* (6), 3388−3393.

(14) Yuan, Q.; Sun, C. Y.; Yang, X.; Ma, P. C.; Ma, Z. W.; Li, Q. P.; Chen, G. J. Gas production from methane-hydrate-bearing sands by ethylene glycol injection using a three-dimensional reactor. *Energy Fuels* **2011**, *25* (7), 3108−3115.

(15) Ota, M.; Morohashi, K.; Abe, Y.; Watanabe, M.; Smith, R. L.; Inomata, H. Replacement of CH_4 in the hydrate by use of liquid CO_2. *Energy Convers. Manage.* **2005**, *46* (11−12), 1680−1691.

(16) Zhou, X. T.; Fan, S. S.; Liang, D. Q.; Du, J. W. Replacement of methane from quartz sand-bearing hydrate with carbon dioxide-in-water emulsion. *Energy Fuels* **2008**, *22* (3), 1759−1764.

(17) Moridis, G. J.; Reagan, M. T. Strategies for Gas Production From Oceanic Class 3 Hydrate Accumulations. In *The Offshore Technology Conference*; Houston, Texas, 2007; Paper OTC 18865.

(18) Li, X. S.; Yang, B.; Li, G.; Li, B.; Zhang, Y.; Chen, Z. Y. Experimental study on gas production from methane hydrate in porous media by huff and puff method in pilot-scale hydrate simulator. *Fuel* **2012**, *94* (1), 486−494.

(19) Sayegh, S. G.; Maini, B. B. Laboratory evaluation of the CO_2 huff-n-puff process for heavy oil-reservoirs. *J. Can. Pet. Technol.* **1984**, *23* (3), 29−36.

(20) Al-Wadhahi, M.; Boukadi, F. H.; Al-Bemani, A.; Al-Maamari, R.; Al-Hadrami, H. Huff 'n puff to revaporize liquid dropout in an Omani gas field. *J. Pet. Sci. Eng.* **2007**, *55* (1−2), 67−73.

(21) Li, G.; Moridis, G. J.; Zhang, K.; Li, X. S. The use of huff and puff method in a single horizontal well in gas production from marine gas hydrate deposits in the Shenhu Area of South China Sea. *J. Pet. Sci. Eng.* **2011**, *77* (1), 49−68.

(22) Li, X. S.; Li, B.; Li, G.; Yang, B. Numerical simulation of gas production potential from permafrost hydrate deposits by huff and puff method in a single horizontal well in Qilian Mountain, Qinghai province. *Energy* **2012**, *40* (1), 59−75.

(23) Yang, X.; Sun, C. Y.; Su, K. H.; Yuan, Q.; Li, Q. P.; Chen, G. J. A three-dimensional study on the formation and dissociation of methane hydrate in porous sediment by depressurization. *Energy Convers. Manage.* **2012**, *56*, 1−7.

(24) Li, X. S.; Zhang, Y.; Li, G.; Chen, Z. Y.; Wu, H. J. Experimental investigation into the production behavior of methane hydrate in porous sediment by depressurization with a novel three-dimensional cubic hydrate simulator. *Energy Fuels* **2011**, *25* (10), 4497−4505.

(25) Li, G.; Li, X. S.; Wang, Y.; Zhang, Y. Production behavior of methane hydrate in porous media using huff and puff method in a novel three-dimensional simulator. *Energy* **2011**, *36* (5), 3170−3178.

(26) Li, X. S.; Wang, Y.; Li, G.; Zhang, Y.; Chen, Z. Y. Experimental investigation into methane hydrate decomposition during three-dimensional thermal huff and puff. *Energy Fuels* **2011**, *25* (4), 1650−1658.

(27) Moridis, G. J.; Kowalsky, M. B.; Pruess, K. *TOUGH+HYDRATE v1.1 User's Manual: A Code for the Simulation of System Behavior in Hydrate-Bearing Geologic Media*; Lawrence Berkeley National Laboratory: Berkeley, CA, 2009.

(28) Li, X. S.; Yang, B.; Zhang, Y.; Li, G.; Duan, L. P.; Wang, Y.; Chen, Z. Y.; Huang, N. S.; Wu, H. J. Experimental investigation into gas production from methane hydrate in sediment by depressurization in a novel pilot-scale hydrate simulator. *Appl. Energy* **2012**, *93*, 722−732.

(29) Moridis, G. J.; Reagan, M. T.; Kim, S. J.; Seol, Y.; Zhang, K. Evaluation of the gas production potential of marine hydrate deposits in the Ulleung Basin of the Korean East Sea. *SPE J.* **2009**, *14* (4), 759−781.

(30) Li, G.; Li, X. S.; Chen, Q.; Chen, Z. Y. Numerical simulation of gas production from gas hydrate zone in Shenhu Area, South China Sea. *Acta Chim. Sin.* **2010**, *68* (11), 1083−1092.

(31) Moridis, G. J.; Reagan, M. T.; Boyle, K. L.; Zhang, K. Evaluation of the Gas Production Potential of Challenging Hydrate Deposits. In *TOUGH Symposium*; Lawrence Berkeley National Laboratory: Berkeley, CA, 2009.

(32) Li, X. S.; Zhang, Y.; Li, G.; Chen, Z. Y.; Yan, K. F.; Li, Q. P. Gas hydrate equilibrium dissociation conditions in porous media using two thermodynamic approaches. *J. Chem. Thermodyn.* **2008**, *40* (9), 1464−1474.

(33) Zhang, K.; Moridis, G. J.; Wu, Y. S.; Pruess, K. A Domain Decomposition Approach for Large-Scale Simulations of Flow Processes in Hydrate-Bearing Geologic Media. In *The 6th International Conference on Gas Hydrate*; Vancouver, British Columbia, Canada, 2008; Paper 5480.

(34) Moridis, G. J.; Collett, T. S.; Dallimore, S. R.; Satoh, T.; Hancock, S.; Weatherill, B. Numerical studies of gas production from several CH_4 hydrate zones at the Mallik site, Mackenzie Delta, Canada. *J. Pet. Sci. Eng.* **2004**, *43* (3−4), 219−238.

(35) Li, G.; Li, B.; Li, X. S.; Zhang, Y.; Wang, Y. Experimental and numerical studies on gas production from methane hydrate in porous media by depressurization in pilot-scale hydrate simulator. *Energy Fuels* **2012**, *26* (10), 6300−6310.

(36) Yousif, M. H.; Abass, H. H.; Selim, M. S.; Sloan, E. D. Experimental and theoretical investigation of methane-gas-hydrate dissociation in porous media. *SPE Reservoir Eng.* **1991**, *6* (4), 69−76.

(37) Moridis, G. J.; Seol, Y.; Kneafsey, T. J. Studies of reaction kinetics of methane hydrate dissociation in porous media. In *The 5th International Conference on Gas Hydrate*; Trondheim, Norway, 2005; pp 1004−1014.

(38) van Genuchten, M. T. A Closed-form equation for predicting the hydraulic conductivity of unsaturated soils. *Soil Sci. Soc. Am. J.* **1980**, *44*, 892−898.